# Efficient implementation of volume/surface integrated average based multi-moment method

Mohammed Al-Mosallam[1] and Kensuke Yokoi[1] *
[1]School of Engineering, Cardiff University,
The Parade, Cardiff, CF24 3AA, UK.

April 15, 2016

**Abstract**

We investigated discretization strategies of the conservation equation in VSIAM3 (volume/surface integrated average based multi-moment method) which is a numerical framework for incompressible and compressible flows based on a multi-moment concept. We investigated these strategies through the lid-driven cavity flow problem, shock tube problems, 2D explosion test and droplet splashing on a superhydrophobic substrate. We found that the use of the CIP-CSLR (constrained interpolation profile-conservative semi-Lagrangian with rational function) method as the conservation equation solver is critically important for the robustness of incompressible flow simulations using VSIAM3 and that numerical results are sensitive to discretization techniques of the divergence term in the conservation equation. Based on these results, we proposed efficient implementation techniques of VSIAM3.

keywords: multi-moment method; VSIAM3; CIP-CSL method; shock tube; droplet splashing

## 1 Introduction

VSIAM3 [23, 24, 28] is a numerical framework to simulate incompressible and compressible flows, and employs a CIP-CSL method [21, 30, 25, 26] as the conservation equation solver. VSIAM3 has been applied to various fluids problems [23, 24, 28] including droplet splashing [38, 39, 40]. In experiences of one of the authors [38, 39, 40], VSIAM3 is a highly robust and efficient numerical framework. However most of researchers who tried to develop the code could not conduct robust fluid simulations [13]. This is because a multi-moment framework which has been used in VSIAM3 (including the CIP-CSL method) has increased some complexities in the implementation and the full detail of the efficient/robust implementation of VSIAM3 has not been described in any paper. The issue on the robustness in VSIAM3 has also been implied in [9] and a possible solution using the simple CIP interpolation for the issue has been proposed. In the paper, we identify the reasons and supply the full details of efficient implement of VSIAM3. Our approach is fully based on VSIAM3 (without using the simple CIP interpolation) and simple.

VSIAM3 and the CIP-CSL methods can be considered as multi-moment methods. Multi-moment methods are defined as methods which use at least two different types of moments (variables) and update these moments by using different formulations (but the same governing equation). For instance, the CIP-CSL2 (CIP-CSL with 2nd-order polynomial function) method [30] which is a solver of the conservation equation uses boundary value (point value in 1D) and cell average as moments (i.e. two different moments). The boundary value and cell average are updated by using finite difference and finite volume formulations, respectively (i.e. two different formulations). VSIAM3 also uses the same moments with these in CSL2. The CIP method [31, 32, 33], IDO (interpolated differential operator) scheme [1] and MCV (multi-moment constrained finite volume) [6] can also be categorized in multi-moment methods. On the

*Corresponding author: School of Engineering, Cardiff University, The Parade, Cardiff, CF24 3AA, UK. Tel: +44 (0)29 20870844, Fax: +44 (0)29 20874716, email:YokoiK@cardiff.ac.uk.

other hand, most of numerical methods in fluids are based on single-moment such as MUSCL (monotonic upwind-centred scheme for conservation laws) [11], ENO (essentially non-oscillatory) [3] and WENO (weighted ENO) [10, 7] (i.e. point value only or cell average only).

The CIP-CSL method is a solver of the conservation equation which is used in VSIAM3. Several CIP-CSL methods such as CSL2 [30], CSL3 [25] and CSLR (CSL with rational function) [26] have been proposed. These CIP-CSL methods are based on a semi-Lagrangian framework. The CIP-CSL methods construct the interpolation functions using only moments (variables) within one cell and increase the order of accuracy by increasing the number of moments in each cell, while single-moment methods increase the order of accuracy by increasing the number of cells which are used in their discretization. In the CIP-CSL2 method, 2nd-order polynomial interpolation function is employed as the interpolation function, and two boundary values and a cell average in the upwind cell were used as the constraints. In CSL3, 3rd-order polynomial interpolation function is employed, and two boundary values and a cell average in the upwind cell are used as the constraints and a gradient in the upwind cell is also used as a control parameter. CSL3 is typically used for compressible flows and the control parameter is used as a limiter. CSLR is a less oscillatory CSL formulation based on rational functions. In this paper, CSL2, CSLR and CSL3 are used and detailed. In this paper, we found that the use of a less oscillatory CSL formulation (CSLR) is critically important for robust incompressible fluid simulations and that the divergence term which appears in these CSL schemes play a key role in the robustness of VSIAM3.

In Section 2, a review of VSIAM3 for incompressible flows is given. We also propose several formulations of the divergence term in Section 2.6. In Section 3, the details of VSIAM3 for compressible flows is given. Numerical results of lid-driven cavity flow, shock tube problems, 2D explosion test and droplet splashing are given in Section 4. The summary comes in Section 5.

# 2 VSIAM3 for incompressible flows

## 2.1 Governing equations

The following governing equations are used for incompressible flow

$$\int_\Gamma \mathbf{u}\cdot\mathbf{n}dS = 0, \tag{1}$$

$$\frac{\partial}{\partial t}\int_\Omega \mathbf{u}dV + \int_\Gamma \mathbf{u}(\mathbf{u}\cdot\mathbf{n})dS = -\frac{1}{\rho}\int_\Gamma p\mathbf{n}dS + \frac{1}{\rho}\int_\Gamma \tau\cdot\mathbf{n}dS, \tag{2}$$

where $\mathbf{u}$ is the velocity, $\mathbf{n}$ the outgoing normal for the control volume $\Omega$ with its surface denoted by $\Gamma$ (see Fig. 1), $\rho$ the density, $p$ the pressure and $\tau$ the viscous stress tensor. A fractional step approach [37] is used to solve the governing equations as follows:

$$\mathbf{u}^{t+\Delta t} = f^{NA2}(f^{NA1}(f^{A}(\mathbf{u}^{t}))), \tag{3}$$

1. advection part ($f^A$):

$$\frac{\partial}{\partial t}\int_\Omega \mathbf{u}dV + \int_\Gamma \mathbf{u}(\mathbf{u}\cdot\mathbf{n})dS = 0, \tag{4}$$

2. non-advection part 1 ($f^{NA1}$):

$$\frac{\partial}{\partial t}\int_\Omega \mathbf{u}dV = \frac{1}{\rho}\int_\Gamma \tau\cdot\mathbf{n}dS, \tag{5}$$

3. non-advection part 2 ($f^{NA2}$):

$$\int_\Gamma \mathbf{u}\cdot\mathbf{n}dS = 0, \tag{6}$$

$$\frac{\partial}{\partial t}\int_\Omega \mathbf{u}dV = -\frac{1}{\rho}\int_\Gamma p\mathbf{n}dS. \tag{7}$$

These equations are solved by VSIAM3, in which the advection part is solved by a CIP-CSL method.

## 2.2 Grid for VSIAM3 (M-grid)

VSIAM3 uses the grid as shown in Fig. 1. This grid is called M-grid [27], and employs cell averages and boundary values as the moments. The cell averages $u_{i,j}, v_{i,j}, p_{i,j}$ are defined at the cell centre and the boundary values $u_{i-1/2,j}$, $u_{i,j-1/2}$ ,$v_{i-1/2,j}$, $v_{i,j-1/2}$ are defined on the cell boundaries. A cell average and boundary values are defined as

$$u_{i,j} = \frac{1}{\Delta x \Delta y} \int_{x_{i-1/2}}^{x_{i+1/2}} \int_{y_{j-1/2}}^{y_{j+1/2}} u(x,y) dx dy, \tag{8}$$

$$u_{i-1/2,j} = \frac{1}{\Delta y} \int_{y_{j-1/2}}^{y_{j+1/2}} u(x_{i-1/2},y) dy, \tag{9}$$

$$u_{i,j-1/2} = \frac{1}{\Delta x} \int_{x_{j-1/2}}^{x_{j+1/2}} u(x,y_{j-1/2}) dx. \tag{10}$$

## 2.3 Advection part ($f^A$)

The CIP-CSL methods are used to solve the conservation equation

$$\frac{\partial}{\partial t} \int_\Omega \phi dV + \int_\Gamma \phi (\mathbf{u} \cdot \mathbf{n}) dS = 0, \tag{11}$$

here $\phi$ is a scalar value. In the following subsections 2.3.1 and 2.3.2, the CIP-CSL2 method [30] and the CIP-CSLR method [26] are explained, respectively.

### 2.3.1 CIP-CSL2

In the CIP-CSL2 method [30], a quadratic interpolation function $\Phi_i(x)$

$$\Phi_i(x) = a_i (x - x_{i-1/2})^2 + b_i (x - x_{i-1/2}) + \phi_{i-1/2}, \tag{12}$$

is used to interpolate between $x_{i-1/2}$ and $x_{i+1/2}$ as shown in Fig. 2, The coefficients, $a_i$ and $b_i$, are determined as follows

$$a_i = \frac{1}{\Delta x^2} (-6\phi_i + 3\phi_{i-1/2} + 3\phi_{i+1/2}), \tag{13}$$

$$b_i = \frac{1}{\Delta x} (6\phi_i - 4\phi_{i-1/2} - 2\phi_{i+1/2}). \tag{14}$$

by using the following constraints

$$\Phi_i(x_{i+1/2}) = \phi_{i+1/2}, \tag{15}$$

$$\phi_i = \int_{x_{i-1/2}}^{x_{i+1/2}} \Phi_i(x) dx / \Delta x. \tag{16}$$

By using the interpolation function $\Phi_i(x)$, the boundary value $\phi_{i-1/2}$ can be updated by the conservation equation of a differential form

$$\frac{\partial \phi}{\partial t} + u \frac{\partial \phi}{\partial x} = -\phi \frac{\partial u}{\partial x}. \tag{17}$$

(17) is solved using a splitting approach as follows

$$\frac{\partial \phi}{\partial t} + u \frac{\partial \phi}{\partial x} = 0, \tag{18}$$

$$\frac{\partial \phi}{\partial t} = -\phi \frac{\partial u}{\partial x}. \tag{19}$$

A semi-Lagrangian approach is used for the advection equation (18)

$$\phi^*_{i-1/2} = \begin{cases} \Phi_{i-1}(x_{i-1/2} - u_{i-1/2}\Delta t) & \text{if} \quad u_{i-1/2} \geq 0 \\ \Phi_i(x_{i-1/2} - u_{i-1/2}\Delta t) & \text{if} \quad u_{i-1/2} < 0. \end{cases} \tag{20}$$

(19) represents a correction due to the divergence term of the velocity and is solved by a finite difference method. The divergence term is one of main topics in this paper as discussed in Section 2.6. The cell average $\phi_i$ is updated by a finite volume formulation

$$\phi_i^{n+1} = \phi_i^n - \frac{1}{\Delta x}(F_{i+1/2} - F_{i-1/2}), \tag{21}$$

here $F_{i-1/2}$ is the flux

$$F_{i-1/2} = \begin{cases} -\int_{x_{i-1/2}}^{x_{i-1/2}-u_{i-1/2}\Delta t} \Phi_{i-1}(x)dx & \text{if} \quad u_{i-1/2} \geq 0 \\ -\int_{x_{i-1/2}}^{x_{i-1/2}-u_{i-1/2}\Delta t} \Phi_i(x)dx & \text{if} \quad u_{i-1/2} < 0. \end{cases} \tag{22}$$

### 2.3.2 CIP-CSLR

The CIP-CSLR [26] method is characterised by less numerical oscillations. Although two CSLR formulations (CSLR0 and CSLR1) have been proposed [26], we explain only CSLR0 here (hereafter CSLR0 is referred to as CSLR in this paper). Instead of (12) in the CIP-CSL2 formulation, the following interpolation function

$$\Phi_i(x) = \frac{\alpha_i\beta_i(x - x_{i-1/2})^2 + 2\alpha_i(x - x_{i-1/2}) + \phi_{i-1/2}}{\left(1 + \beta_i(x - x_{i-1/2})\right)^2}, \tag{23}$$

with

$$\alpha_i = \beta_i\phi_i + (\phi_i - \phi_{i-1/2})/\Delta x, \tag{24}$$

$$\beta_i = \frac{1}{\Delta x}\left(\frac{|(\phi_{i-1/2} - \phi_i)| + \varepsilon}{|(\phi_i - \phi_{i+1/2})| + \varepsilon} + 1\right), \tag{25}$$

is used. Here $\varepsilon$ is an infinitesimal number to avoid zero division. We used $\varepsilon = 10^{-16}$ for all results in this paper. All other procedures are the same with these in CSL2.

### 2.3.3 Multi-dimensional cases

For multi-dimensional cases, a dimensional splitting method [23] is used. For x-direction, $\phi^*_{i,j}$ and $\phi^*_{i-1/2,j}$ are firstly computed from $\phi^n_{i,j}$ and $\phi^n_{i-1/2,j}$ by using 1D CIP-CSL solver. However $\phi^n_{i,j-1/2}$ cannot be updated by using 1D CIP-CSL solver. Therefore $\phi^n_{i,j-1/2}$ is updated by TEC (Time Evolution Converting) as follows:

$$\phi^*_{i,j-1/2} = \phi^n_{i,j-1/2} + \frac{1}{2}(\phi^*_{i,j} - \phi^n_{i,j} + \phi^*_{i,j-1} - \phi^n_{i,j-1}). \tag{26}$$

A similar approach is used for y-direction. $\phi^{n+1}_{i,j}$ and $\phi^{n+1}_{i,j-1/2}$ are computed from $\phi^*_{i,j}$ and $\phi^*_{i-1/2,j}$ by using a 1D CIP-CSL method. $\phi^*_{i-1/2,j}$ is updated by TEC as follows:

$$\phi^{n+1}_{i-1/2,j} = \phi^*_{i-1/2,j} + \frac{1}{2}(\phi^{n+1}_{i,j} - \phi^*_{i,j} + \phi^{n+1}_{i-1,j} - \phi^*_{i-1,j}). \tag{27}$$

## 2.4 Non-advection Part 1 ($f^{NA1}$)

The viscosity term is computed by a standard finite volume formulation for cell averages.

$$\frac{1}{\rho}\int_\Gamma \tau \cdot \mathbf{n} dS = \frac{1}{\rho_{i,j}}\left(\frac{\tau_{i+1/2,j} - \tau_{i-1/2,j}}{\Delta x} + \frac{\tau_{i,j+1/2} - \tau_{i,j-1/2}}{\Delta y}\right). \tag{28}$$

The boundary values are updated by TEC.

## 2.5 Non-advection Part 2 ($f^{NA2}$)

By using the divergence of (7) and $\int_\Gamma \mathbf{u}^{n+1}\cdot\mathbf{n}dS = 0$, the following Poisson equation

$$\int_\Gamma \frac{\nabla p^{n+1}}{\rho}\cdot\mathbf{n}dS = \frac{1}{\Delta t}\int_\Gamma \mathbf{u}^*\cdot\mathbf{n}dS, \tag{29}$$

is obtained, where $\mathbf{u}^*$ is the velocity after non-advection part 1. (29) is discretized as

$$\begin{aligned}&\frac{(\frac{1}{\rho^{n+1}_{i+1/2,j}}\partial_x p^{n+1})_{i+1/2,j} - (\frac{1}{\rho^{n+1}_{i-1/2,j}}\partial_x p^{n+1})_{i-1/2,j}}{\Delta x}\\ +&\frac{(\frac{1}{\rho^{n+1}_{i,j+1/2}}\partial_y p^{n+1})_{i,j+1/2} - (\frac{1}{\rho^{n+1}_{i,j-1/2}}\partial_x p^{n+1})_{i,j-1/2}}{\Delta y}\\ =&\frac{1}{\Delta t}(\frac{u^*_{i+1/2,j}-u^*_{i-1/2,j}}{\Delta x}+\frac{v^*_{i,j+1/2}-v^*_{i,j-1/2}}{\Delta y}),\end{aligned} \tag{30}$$

here

$$(\frac{1}{\rho^{n+1}_{i-1/2,j}}\partial_x p^{n+1})_{i-1/2,j} \equiv \frac{2}{\rho^{n+1}_{i,j}+\rho^{n+1}_{i-1,j}}\frac{p^{n+1}_{i,j}-p^{n+1}_{i-1,j}}{\Delta x}. \tag{31}$$

A preconditioned conjugate gradient (CG) method [4] is used for the pressure Poisson equation. The convergence tolerance of the pressure Poisson equation $\varepsilon_p = 10^{-10}$ is used. By using $p^{n+1}$, the boundary values of the velocity are updated as follows ($u_{i-1/2,j}$, $v_{i,j-1/2}$)

$$u^{n+1}_{i-1/2,j} = u^*_{i-1/2,j} - \frac{\Delta t}{\rho_{i-1/2,j}}\left(\partial_x p^{n+1}\right)_{i-1/2,j}, \tag{32}$$

$$v^{n+1}_{i,j-1/2} = v^*_{i,j-1/2} - \frac{\Delta t}{\rho_{i,j-1/2}}\left(\partial_y p^{n+1}\right)_{i,j-1/2}. \tag{33}$$

Other velocity components ($u_{i,j}$, $v_{i,j}$, $u_{i,j-1/2}$, $v_{i-1/2,j}$) are updated by the TEC formula.

## 2.6 Formulations of the divergence term

As we mentioned in Section 2.3, in this section, we explain how to discretize the divergence term (19) of the 1D conservation equation.

**Simple central difference based on boundary value (CDb)**

$$\phi\frac{\partial u}{\partial x} = \phi^*_{i-1/2}\frac{u^n_{i+1/2}-u^n_{i-3/2}}{2\Delta x}. \tag{34}$$

In the original papers of the CIP-CSL methods [30, 25], the simple central difference approximation using boundary values has been suggested.

In this paper, we propose the following approximations of the velocity divergence term.

**Simple upwind based on boundary value (UPW)**

$$\phi\frac{\partial u}{\partial x} = \begin{cases}\phi^*_{i-1/2}(\frac{u^n_{i-1/2}-u^n_{i-3/2}}{\Delta x}) & \text{if} \quad u_{i-1/2} > 0\\ \phi^*_{i-1/2}(\frac{u^n_{i+1/2}-u^n_{i-1/2}}{\Delta x}) & \text{if} \quad u_{i-1/2} \le 0.\end{cases} \tag{35}$$

This is a simple upwind approximation based on the boundary values.

**Central difference based on cell average (CDca)**

$$\phi \frac{\partial u}{\partial x} = \phi^*_{i-1/2} \frac{u^n_i - u^n_{i-1}}{\Delta x}. \tag{36}$$

This is a central difference formula based on the cell averages. Compared to CDb (34), the proposed central difference formulation employs the cell average instead of the boundary values, and the stencil is shorter than that of CDb.

**Central difference based cell centre value (CDcc)**

$$\phi \frac{\partial u}{\partial x} = \phi^*_{i-1/2} \frac{\hat{u}^n_i - \hat{u}^n_{i-1}}{\Delta x} \tag{37}$$

This is another central difference approximation based on the cell center values ($\hat{u}_i$), where $\hat{u}_i$ is the velocity calculated at cell centre [25]. By using the quadratic function (12), $\hat{u}_i$ can be obtained

$$\hat{u}_i = \frac{3}{2} u_i - \frac{1}{4} \left( u_{i+1/2} + u_{i-1/2} \right). \tag{38}$$

**Central difference based on a 4th-order polynomial function (CDbca)**

$$\phi \frac{\partial u}{\partial x} = \phi^*_{i-1/2} \left( 2 \frac{u^n_i - u^n_{i-1}}{\Delta x} - \frac{u^n_{i+1/2} - u^n_{i-3/2}}{2\Delta x} \right). \tag{39}$$

This formula (39) can be derived from a fourth-order central interpolation function using $u_{i-3/2}$, $u_{i-1}$, $u_{i-1/2}$, $u_i$ and $u_{i+1/2}$ [12].

**Mixed formulation of the simple upwind and a central difference (UPW-CDcc)**

$$\phi \frac{\partial u}{\partial x} = \begin{cases} \mathrm{D}_{UPW} & \text{if} \quad \mathrm{D}_{UPW} \cdot \mathrm{D}_{CDcc} < 0 \\ \mathrm{D}_{UPW} & \text{else if} \quad |\mathrm{D}_{UPW}| < |\mathrm{D}_{CDcc}| \\ \mathrm{D}_{CDcc} & \text{else,} \end{cases} \tag{40}$$

here $\mathrm{D}_{UPW}$ and $\mathrm{D}_{CDcc}$ represent $\phi \frac{\partial u}{\partial x}$ which are calculated by (35) and (37), respectively. The mixed formulation is introduced to take advantages of both upwind and central difference approximations. The formulation employs the upwind formula (35) when the sign of derivatives of UPW and CDcc are different ($\mathrm{D}_{UPW} \cdot \mathrm{D}_{CDcc} < 0$) or $|\mathrm{D}_{CDcc}|$ is larger than that of $|\mathrm{D}_{UPW}|$. Otherwise the central difference formula (37) is used. Although we combined UPW with CDcc in this paper, it can be combined with any other central difference formulations. In this paper, we also combined UPW with CDbca (UPW-CDbca).

**Interpolation at characteristic departure point (DP)**

$$\phi \frac{\partial u}{\partial x} = \begin{cases} \phi^*_{i-1/2} \dfrac{\partial \Phi_{i-1}}{\partial x}(x_{i-1/2} - u_{i-1/2}\Delta t) & \text{if} \quad u_{i-1/2} \geq 0 \\ \phi^*_{i-1/2} \dfrac{\partial \Phi_i}{\partial x}(x_{i-1/2} - u_{i-1/2}\Delta t) & \text{if} \quad u_{i-1/2} < 0. \end{cases} \tag{41}$$

This formulation evaluates the divergence at the characteristic departure point using a CIP-CSL interpolation function.

## 2.7 Formulations of the divergence term in Fourier analysis

In this section, we conduct Fourier analysis of these divergence term formulations. Fourier analysis shows resolution of spatial derivatives in the wavenumber domain. The spatial profile of the velocity $U(x)$ is defined over the domain [0, L] with a uniform grid spacing $\Delta x$ is decomposed into Fourier series

$$U(x) = \sum_{\kappa} U(\kappa) e^{j\omega x/\Delta x}, \tag{42}$$

where $j = \sqrt{-1}$ and $\omega = 2\pi\kappa\Delta x/L$ is the scaled wavenumber. The point value at $x_{i-1/2}$ is also decomposed as

$$u_{i-1/2} = \sum_{\kappa} U(\kappa) e^{j\omega x_{i-1/2}/\Delta x}. \tag{43}$$

Using (43), the point value at $x_{i-1/2+m}$ is decomposed as

$$u_{i-1/2+m} = u_{i-1/2} e^{j\omega m}. \tag{44}$$

The cell average $u_i$ is also decomposed as

$$u_i = \frac{1}{\Delta x}\int_0^{\Delta x} U(x_{i-1/2}+x)dx = u_{i-1/2}\frac{e^{j\omega}-1}{j\omega} \tag{45}$$

Since equation (45) expresses the relation between the point value and the cell average, the accuracy of the proposed formulations of the divergence term can be examined by using (44) and (45). The formulations of divergence term in Fourier space are obtained as follows

$$U_{x,CDb}(\omega) = j(\sin(\omega)), \tag{46}$$

$$U_{x,UPW}(\omega) = (\cos(\omega)-1) + j(\sin(\omega)), \tag{47}$$

$$U_{x,CDca}(\omega) = j(\sin(\omega)), \tag{48}$$

$$U_{x,CDcc}(\omega) = j(\frac{6\sin^2(\omega/2)}{\omega} - \frac{\sin(\omega)}{2}), \tag{49}$$

$$U_{x,CDbca}(\omega) = j(-\sin(\omega) + \frac{8\sin^2(\omega/2)}{\omega}). \tag{50}$$

$U_{x,DP}$ depends on the interpolation function of a CSL method. However, in this paper, CSLR and CSL3 are mainly used and both CSL methods are using nonlinear interpolation function. Therefore we cannot analyze DP formulation.

Fig. 3 shows the results of various formulations of the divergence term in Fourier space. All central difference methods have no error in real part (no diffusion error) and only UPW has diffusion error, as shown in Fig. 3 (b). Fig. 3 (a) has shown that CDbca is the closest to the exact solution. CDcc is second closest, CDca third, CDca fourth, and CDb and UPW are the most inaccurate.

# 3 VSIAM3 framework for inviscid compressible flows

## 3.1 Governing equations

The Euler equations describe the dynamics of inviscid compressible flows and are written as

$$\frac{\partial U}{\partial t} + \frac{\partial F(U)}{\partial x} = 0, \tag{51}$$

where

$$U = \left\{ \begin{array}{c} \rho \\ m \\ E \end{array} \right\}, \tag{52}$$

$$F(U) = \left\{ \begin{array}{c} m \\ um + p \\ Eu + pu \end{array} \right\}, \tag{53}$$

where $m$ is the momentum ($m=\rho u$) and E the total energy. The equations are completed by the equation of state

$$p=\left(E-\frac{\rho u^2}{2}\right)(\gamma-1), \tag{54}$$

where $\gamma$ is the specific heat ratio. By using the VSIAM3 formulation [24], (53) is split into two parts, advection part and non-advection part

$$F(U)=F^I(U)+F^{II}(U)=\left\{\begin{array}{c} m \\ um \\ Eu \end{array}\right\}+\left\{\begin{array}{c} 0 \\ p \\ pu \end{array}\right\}. \tag{55}$$

A fractional step approach is used to solve (51), in which the advection part

$$\frac{\partial U}{\partial t}+\frac{\partial F^I(U)}{\partial x}=0, \tag{56}$$

is solved by CIP-CSL3 method [25]. The non-advection part

$$\frac{\partial U}{\partial t}+\frac{\partial F^{II}(U)}{\partial x}=0, \tag{57}$$

is solved by finite volume/difference formulations.

## 3.2 Advection part: CIP-CSL3

The CIP-CSL3 method is an extension of the CIP-CSL2 method. In this method, 3rd-order polynomial function is employed as the interpolation function instead of the quadratic function of CSL2. Then CSL3 needs one more constraint to determine all coefficients and introduces a control parameter (gradient at the cell center) as the additional constraint. The control parameter can be used as slope limiter to eliminate numerical oscillation [24]. The 3rd-order polynomial interpolation function between $x_{i-1/2}$ and $x_{i+1/2}$ is written as

$$\Phi_i(x)=a_i(x-x_{i-1/2})^3+b_i(x-x_{i-1/2})^2+c_i(x-x_{i-1/2})+\phi_{i-1/2}. \tag{58}$$

In addition to the constraints (15) and (16), the following constraint

$$\frac{d\Phi_i(x_i)}{dx}=d_i, \tag{59}$$

is used to determine the coefficients of (58) as follows

$$a_i=\frac{4\left(\phi_{i+1/2}-\phi_{i-1/2}-\Delta x d_i\right)}{\Delta x^3}, \tag{60}$$

$$b_i=\frac{3\left(-2\phi_i-\phi_{i+1/2}+3\phi_{i-1/2}+2\Delta x d_i\right)}{\Delta x^2}, \tag{61}$$

$$c_i=\frac{2\left(3\phi_i-3\phi_{i-1/2}-\Delta x d_i\right)}{\Delta x}. \tag{62}$$

The derivative $d_i$ is given as

$$d_i=\beta_i\tilde{d}_i, \tag{63}$$

$$\tilde{d}_i=\mathrm{minmod}\left(\frac{S_{i+1/2}+S_{i-1/2}}{2},2S_{i+1/2},2S_{i-1/2}\right), \tag{64}$$

here

$$\mathrm{minmod}(A,B,C)=\left\{\begin{array}{ll} \mathrm{m}(A,B,C) & \text{if} \quad \mathrm{sgn}(A)=\mathrm{sgn}(B)=\mathrm{sgn}(C) \\ 0 & \text{otherwise,} \end{array}\right. \tag{65}$$

$$m(A,B,C) = \begin{cases} A & \text{if} \quad \min(|A|,|B|,|C|) = |A| \\ B & \text{else if} \quad \min(|A|,|B|,|C|) = |B| \\ C & \text{else} \quad \min(|A|,|B|,|C|) = |C|, \end{cases} \tag{66}$$

and

$$S_{i-1/2} = \frac{\hat{\phi}_i - \hat{\phi}_{i-1}}{\Delta x}, \tag{67}$$

where

$$\hat{\phi}_i = \frac{3}{2}\phi_i - \frac{1}{4}(\phi_{i+1/2} + \phi_{i-1/2}), \tag{68}$$

and

$$\beta_i = \begin{cases} 0.0125 & \text{if} \quad (u^n_{i-1/2} - u^n_{i+1/2}) < 0.02\Delta x \\ 1.2 & \text{otherwise.} \end{cases} \tag{69}$$

Given at time step n, the cell averages, $\rho^n_i$, $u^n_i$, $p^n_i$, $m^n_i$, $E^n_i$ and the cell boundary values $\rho^n_{i-1/2}$, $u^n_{i-1/2}$, $m^n_{i-1/2}$, $E^n_{i-1/2}$, the CIP-CSL3 method is used to obtain the corresponding density at the next time step n+1 (i.e. $\rho^{n+1}_i$ and $\rho^{n+1}_{i-1/2}$) and the provisional values of the momentum and energy (i.e. $m^*_i$, $m^*_{i-1/2}$, $E^*_i$ and $E^*_{i-1/2}$).

### 3.3 The Non-advection Phase

A simple explicit equation [24] is used to advance the pressure

$$p^{n+1}_i = C_i^2 \Delta t \left( u^*_i \frac{\rho^{n+1}_{i+1/2} - \rho^{n+1}_{i-1/2}}{\Delta x} + \frac{\rho^{n+1}_i}{\gamma \Delta t} - \frac{m^*_{i+1/2} - m^*_{i-1/2}}{\Delta x} \right), \tag{70}$$

here $u^*_i = \frac{m^*_i}{\rho^{n+1}_i}$, and, $C_i^2 = \frac{\gamma p^*_i}{\rho^{n+1}_i}$. The boundary values of the momentum and total energy are updated as follows

$$m^{n+1}_{i-1/2} = m^n_{i-1/2} - \frac{\Delta t}{\Delta x}\left(p^{n+1}_i - p^{n+1}_{i-1}\right), \tag{71}$$

$$E^{n+1}_{i-1/2} = E^n_{i-1/2} - \frac{\Delta t}{\Delta x}\left(u^{n+1}_i p^{n+1}_i - u^{n+1}_{i-1} p^{n+1}_{i-1}\right). \tag{72}$$

The cell averages of the momentum and total energy can be obtained via TEC formula as follows

$$m^{n+1}_i = m^n_i + \frac{1}{2}\left(m^{n+1}_{i+1/2} - m^n_{i+1/2} + m^{n+1}_{i-1/2} - m^n_{i-1/2}\right), \tag{73}$$

$$E^{n+1}_i = E^n_i + \frac{1}{2}\left(E^{n+1}_{i+1/2} - E^n_{i+1/2} + E^{n+1}_{i-1/2} - E^n_{i-1/2}\right). \tag{74}$$

For numerical simulations of compressible flows, CSL3 should be used. Although CSLR is also a less oscillatory CSL formulation, CSLR does not include a slope limiter so that CSLR cannot prevent oscillation around shock in VSIAM3 (see Appendix A for some numerical results by CSLR).

## 4 Numerical results

### 4.1 Lid-driven cavity flow

We examined the discretization strategies of the conservation equation through the lid-driven cavity flow problem [2]. The tests were carried out at Reynolds number Re= 1000 and 5000.

Fig. 4a shows the result of Re= 1000 by the CIP-CSL2 method with the simple upwind (UPW). The result shows the x-component of velocity along the vertical line through the centre of cavity. The result shows a reasonable agreement with the solution by Ghia [2]. However the calculation was not stable after obtaining the steady state solution.

Although we also tested CSL2 with central difference approximations, these were not stable and did not reach to the steady state solution. Fig. 4b shows the result when the divergence term was ignored. Although the result was inaccurate, the calculation was stable. These results suggest that the use of the CSL2 in VSIAM3 affects the robustness and the divergence term is relevant to the robustness.

We also examined the use of the CIP-CSLR method in VSIAM3. The numerical results of the CIP-CSLR method with all divergence term approximations are presented in Figures 5 with grid refinement studies using three grid sizes ($50\times50$, $100\times100$ and $200\times200$). All numerical results show reasonable agreements with the Ghia solution and also reasonable convergences. All numerical simulations using CSLR (with any divergence term approximation) were stable in this test problem. These results by CSL2 and CSLR suggest that the use of CSLR improves the robustness of VSIAM3. As explained in section 2.3.2 and [26], CSLR is a less oscillatory formulation and CSL2 is not free from numerical oscillations. Therefore it can be considered that the use of a less oscillatory formulation is critically important for the robustness of VSIAM3 and the numerical oscillations generated by CSL2 affect the robustness in VSIAM3 through the divergence term.

Fig.5b shows the result by UPW. The result is almost equivalent to that of the upwind with a time average approximation given in [23]. The numerical results of the central difference approximations are shown in Figures 5a,c,d and e. These results show that central difference approximations are superior to UPW in this test problem. Although all central difference formulations give similar results, CDbca and CDcc are slightly better than CDb and CDca as shown in Fig. 6 (enlarged figure). It is hardly seen the difference between the results by CDbca and CDcc. CDb is superior to CDca in this test. The result by mixed formulation (UPW-CDcc) is given in Fig. 5f. Fig. 7 shows a comparison among UPW, CDcc and UPW-CDcc. The result by UPW-CDcc is closer to the Ghia solution than that by UPW. Although the results by UPW-CDbca are not presented in this paper, the results by UPW-CDbca show almost identical results with these by UPW-CDcc. In this test problem, the mixed formulation has no advantage for central difference approximations. However, as explained in Section 4.3, the mixed formulation plays an important role in complicated/difficult problems like droplet splashing. The result by DP is better than that by UPW but worse than these by central diference methods in this test as shown in Figures 5 and 6.

Fig. 8 shows numerical simulations of Re$=$ 5000 by CSLR. The trend is almost same with the results of Re=1000.

## 4.2 Compressible flows (Sod's and Lax's problems, and 2D explosion test)

We validate the effects of various discretization techniques for the divergence term in the conservation equation through benchmark problems in compressible fluids, Sod's problem [16] and Lax's problem [8]. The initial condition of Sod's problem is

$$(\rho,u,p)=\begin{cases}(1.0,0,1.0) & \text{if} \quad x\le 0\\ (0.125,0,0.1) & \text{if} \quad x>0.\end{cases} \tag{75}$$

The initial condition of Lax's problem is

$$(\rho,u,p)=\begin{cases}(0.445,0.698,3.528) & \text{if} \quad x\le 0\\ (0.5,0,0.571) & \text{if} \quad x>0.\end{cases} \tag{76}$$

All computations were conducted on a 400-point uniform grid. The numerical results of Sod's and Lax's problems are presented in Figures 9 and 10, respectively. Table 1 shows $L_1$ errors in Sod's and Lax's problems.

Numerical results of Sod's problem by all divergence formulations excluding DP are similar as shown in Fig. 9. DP was not stable for this problem. Table 1 shows that CDbca is the most accurate in Sod's problem and UPW is the worst, in terms of $L_1$ errors. All other central difference approximations (CDb, CDca and CDcc) show very similar errors ($2.24\times10^{-3}-2.25\times10^{-3}$). Mixed formulations (UPW-CDcc and UPW-CDbca) have intermediate errors between UPW and CDcc (or CDbca).

In Lax's problem, we can observe some differences especially around the contact discontinuity as shown in Fig. 10. As shown in Fig. 10 and Table 1, the result by CDb is the worst. This is because Lax's problem involves the discontinuity in the velocity initial condition and the simple central difference formulation (CDb) which uses a wider stencil cannot manege such discontinuity well. Although DP could simulate Lax's problem, it was the second worst. This will be because of the strong discontinuity in the initial condition. Although CDbca was the most accurate in

Sod's problem (which does not involve the discontinuity in the initial velocity condition), second worst in central difference methods. This will also be because CDbca uses a wider stencil like CDb. On the other hand, CDcc is the most accurate and CDca second best in Lax's problem. This will be because CDcc and CDca use a shorter stencil than CDb and CDbca. UPW is less accurate than CDcc and CDca but more accurate than CDb and CDbca, and has a tiny numerical oscillation around the shock (the similar oscillation has also been observed in the previous work by Xiao [24]). If the mixed formulation is used, the tiny oscillation which appears in the numerical result by UPW disappears and numerical diffusion immediately before/after discontinuities, which is observed in numerical results by all central difference approximations is also reduced. Although the mixed formulation shows some improvements, the results by CDcc and CDca are still more accurate in terms of $L_1$ error because the mixed formulation is slightly more diffusive on the discontinuities.

We also conducted numerical simulations of 2D compressible flow (2D exploion test) [22] on the domain $[-1,1] \times [-1,1]$. The initial condition of the 2D explosion problem is

$$\begin{array}{llllll} \rho(x,y,0)=1; & u(x,y,0)=0; & v(x,y,0)=0; & p(x,y,0)=1; & \text{if } r<0.5 \\ \rho(x,y,0)=0.125; & u(x,y,0)=0; & v(x,y,0)=0; & p(x,y,0)=0.1; & \text{otherwise,} \end{array} \tag{77}$$

where $r=\sqrt{x^2+y^2}$. The inviscid Euler conservation laws are solved on a $200 \times 200$ Cartesian grid. Fig. 11 shows the perspective view of the density at t=0.25. These divergence formulations can easily be applied to multi-dimensional fluid problems and the trend is alsmost same with that in Sod's problem.

### 4.3 Droplet splashing

We also conducted numerical simulations of droplet splashing on a superhydrophobic substrate to study the effects of these discretization strategies of the conservation equation in VSIAM3 through a highly complicated free surface flow problem. The numerical formulation to simulate free surface flows is based on VSIAM3. Additionally, for the motion of liquid interface, the CLSVOF (coupled level set and volume-of-fluid) method [18, 34] using both the level set method [14, 17] and the VOF method [15] is used. We use the THINC/WLIC (tangent of hyperbola for interface capturing/weighed line interface calculation) scheme [29, 36] as a type of VOF method. For the surface tension force, the density scaled balanced continuum surface force model with level set curvature correction [39, 40, 41] is used. To impose contact angle, we use a method developed by Sussman [19, 35]. We simulate not only the liquid but also the air. For more detail see [37, 39].

In the set of numerical simulations, quantitative parameters, the densities $\rho_{liquid} = 1000$ kg/m$^3$, $\rho_{air} = 1.25$ kg/m$^3$, viscosities $\mu_{liquid} = 1.0 \times 10^{-3}$ Pa·s, $\mu_{air} = 1.82 \times 10^{-5}$ Pa·s, surface tension $\sigma = 7.2 \times 10^{-2}$ N/m, gravity 9.8 m/s$^2$, initial droplet diameter $D = 1.86$ mm, impact speed 2.98 m/s and the equilibrium contact angle 163$^\circ$ are used. A regular Cartesian grid system of $192 \times 192 \times 48$ is used.

Fig. 12 shows the results. VSIAM3 with CSL2-UPW could not capture droplet splashing well as shown in Fig. 12a. CSL2-UPW also caused relatively large amount of flotsam and was not stable after around 1.1 ms. VSIAM3 with CSL2 with any central difference formulation was not stable for this problem. VSIAM3 with CSLR is stable when UPW was used for the divergence term. The formulation could capture droplet splashing well as shown in Fig. 12b. However if we use any central difference formulation for the divergence term, VSIAM3 with CSLR was also unstable. If we use UPW-CDcc (mixed formulation), VSIAM3 with CSLR could conduct stable numerical simulation of droplet splashing and capture droplet splashing well as shown in Fig. 12c.

## 5 Summary

We investigated discretization strategies of the conservation equation for efficient implementation of VSIAM3 through the lid-driven cavity flow, shock tube problems and droplet splashing.

We examined VSIAM3 with CSL2 and with CSLR through the lid-driven cavity flow and droplet splashing. The numerical results showed that VSIAM3 with CSL2 is not robust enough and that VSIAM3 with CSLR is highly robust (if an appropriate formulation is used for the divergence term). These results indicate that the use of a less oscillatory formulation (i.e. CSLR) is a key for robust incompressible flow simulations.

We also found that the numerical results are sensitive depending on discretization formulations of the divergence term in the conservation equation. The numerical results of the lid-driven cavity flow showed that CSLR with central difference formulations are superior to the simple upwind formulation in this test. However both results are reasonably precise. On the other hand, the numerical results of droplet splashing showed that VSIAM3 with any central difference formulation is not robust even though CSLR is used, while VSIAM3 with the simple upwind formulation was highly robust and captures the droplet splashing well. These results indicates that the use of the upwind formulation is suitable for robust numerical simulations, especially for highly complicated flows like droplet splashing. Although the central difference formulations are precise for simple flow problems such as the cavity flow, will not be robust enough for highly complicated flow problems.

Based on the numerical results, we also proposed the mixed formulation using both a central difference and the simple upwind formulation for the divergence term. The mixed formulation can simulate the lid-driven cavity well (better than UPW and slightly worse than CDcc) and also simulate droplet splashing like the result using the simple upwind. The mixed formulation can take advantages of both central difference and upwind formulations. We summarize the results of incompressible results in Table 2.

We also tested formulations for the divergence term through the inviscid compressible flow problems (Sod's and Lax's problems and 2D explosion test). In Sod's problem which does not involve discontinuity in the velocity initial condition, we could not observe much difference in numerical results by all divergence formulations excluding DP and DP was not stable. In Lax's problem which involves the discontinuity in the velocity initial condition, we could observe some differences especially around the contact discontinuity. In this test, CDb and CDbca, which use a wider stencil were less accurate and CDcc and CDca, which use a shorter stencil were more accurate. The mixed formulation shows some improvements compared to numerical results by any central difference or UPW. However, in terms of $L_1$ error, CDcc and CDca are still better than UPW-CDcc.

In conclusion, employing a less oscillatory CSL scheme (i.e. CSLR, CSL3, etc.) with an appropriate divergence term formulation is critically important for robust implementation of VSIAM3.

# 6 Acknowledgments

This work was partially supported by the Ministry of Higher Education and Scientific Research-Iraq, and College of Engineering in University of Basrah. The numerical simulations were partially conducted on computers at Earth Simulator Center in JAMSTEC, at Yukawa Institute of Theoretical Physics in Kyoto University and at HPC Wales.

# A Sod's and Lax's problems by the CIP-CSLR method

Fig. 13 shows numerical results of Sod and Lax problems by CSLR. CSLR does not include a slope limiter so that numerical oscillations around shock cannot be suppressed in VSIAM3 framework.

# References

[1] T. Aoki, Interpolated differential operator (IDO) scheme for solving partial differential equations, Computer Physics Communications, **102**, 132146 (1997).

[2] U. Ghia, K. N. Ghia, C.T. Shin , High-Re solutions for incompressible flow using the Navier-Stokes equations and a multigrid method, J. Comp. Phys., **48**, 387-411 (1982).

[3] A. Harten and S. Osher, Uniformly high order accurate non-oscillatory schemes, I, SIAM J. Numer. Anal. 24, 279 (1987)

[4] M. R. Hestenes, E. Stiefel, Methods of Conjugate Gradients for Solving Linear Systems, Journal of research of the National Bureau of Standards , **49**, No. 6, Research Paper 2379 (1952).

[5] M. Ida, A conservative semi-Lagrangian method for oscillation-free computation of advection processes, Computer Physics Communications, **143**, 142-154 (2002).

[6] S. Ii, F. Xiao, High order multi-moment constrained finite volume J. Comp. Phys., **228**, 36693707 (2009).

[7] G-S. Jiang, C-W. Shu, Efficient Implementation of Weighted ENO Schemes, J. Comp. Phys., **126**, 202228 (1996).

[8] P. D. Lax, Weak solutions of nonlinear hyperbolic equations and their numerical computation, Comm. Pure Appl. Math.,**7**, 159193 (1954).

[9] S. Lee, I. K. Park, J. J. Jeong, Modified CIP-CSL FV method for incompressible flows, Computers & Fluids, **86**, 240-250 (2013).

[10] X.D. Liu, S. Osher, T. Chan, Weighted essentially non-oscillatory schemes, J. Comput. Phys. 115, 200 (1994).

[11] B. van Leer, Towards the ultimate conservative difference scheme. V. A second-order sequel to Godunov's method, J. Comput. Phys., **32**, 101-136 (1979).

[12] N. Onodera, T. Aoki, H. Kobayashi, Large-eddy simulation of turbulent channel flows with conservative IDO scheme, J. Comput. Phys., **230**, 57875805 (2011).

[13] N. Onodera, et al. (Private communication).

[14] S. Osher and J.A. Sethian, Front propagating with curvature-dependent speed: Algorithms based on Hamilton-Jacobi formulation, J. Comput. Phys. **79**, 12-49 (1988).

[15] R. Scardovelli, S. Zaleski, Direct numerical simulation of free-surface and interfacial flow, Annu. Rev. Fluid Mech., **31**, 567-603 (1999).

[16] G. A. Sod, A Survey of Several Finite Difference Methods for Systems of Non-Linear Hyperbolic Conservation Laws, J. Comput. Phys., **27**, 1-31 (1978).

[17] M. Sussman, P. Smereka, S. Osher, A Level Set Approach for Capturing Solution to Incompressible Two-Phase Flow, J. Comput. Phys. **114**, 146-159 (1994).

[18] M. Sussman, E.G. Puckett., A Coupled Level Set and Volume-of-Fluid Method for Computing 3D and Axisymmetric Incompressible Two-Phase Flows, J. Comput. Phys., **162**, 301-337 (2000).

[19] M. Sussman, An adaptive mesh algorithm for free surface flows in general geometries, in Adaptive Method of Lines, (Chapman & Hall/CRC, Boca Raton, 2002).

[20] H. Takewaki, A. Nishiguchi, T. Yabe, Cubic interpolated pseudo-particle method (CIP) for solving hyperbolic-type equations, J. Comput. Phys.,**61**, 261-268 (1985).

[21] R. Tanaka, T. Nakamura and T. Yabe, Constructing exactly conservative scheme in a non-conservative form, Comput. Phys. Commun., **126**, 232-243 (2000).

[22] E. Toro, Riemann Solvers and Numerical Methods for Fluid Dynamics, Springer, Berlin, 1997.

[23] F. Xiao, A. Ikebata, T. Hasegawa, Numerical simulations of free-interface fluids by a multi-integrated moment method, Computers and Structures, **83**, 409-423 (2005).

[24] F. Xiao, Unified formulation for compressible and incompressible flows by using multi-integrated moments I: one-dimensional inviscid compressible flow, J. Comput. Phys., **195**, 629654 (2004) .

[25] F. Xiao, T. Yabe, Completely Conservative and Oscillationless Semi-Lagrangian Schemes for Advection Transportation, J. Comput. Phys., **170**, 498522 (2001).

[26] F. Xiao, T. Yabe, X. Peng, H. Kobayashi, Conservative and oscillation-less atmospheric transport schemes based on rational functions, J. Geophys. Res., **107** ( D22), 4609, doi:10.1029/2001JD001532, (2002).

[27] F. Xiao, X. D. Peng, X. S. Shen, A Finite-Volume Grid Using Multimoments for Geostrophic Adjustment, Mon. Wea. Rev., **134**, 2515-2526 (2006).

[28] F. Xiao, R. Akoh, S. Ii, Unified formulation for compressible and incompressible flows by using multi-integrated moments II: Multi-dimensional version for compressible and incompressible flows, J. Comp. Phys., **213**, 3-56 (2006).

[29] F. Xiao, Y. Honma, T. Kono, A simple algebraic interface capturing scheme using hyperbolic tangent function, Int. J. Numer. Meth. Fluid., **48**, 1023-1040 (2005).

[30] T. Yabe, R. Tanaka, T. Nakamura, F. Xiao, An Exactly Conservative Semi-Lagrangian Scheme (CIPCSL) in One Dimension, Mon. Wea. Rev.,**129**, 332-344 (2001).

[31] T. Yabe., T. Aoki, A universal solver for hyperbolic equations by cubic-polynomial interpolation I. One-dimensional solver, Computer Physics Communications,**66**, 219232 (1991).

[32] T. Yabe, T. Ishikawa, P.Y. Wang, T. Akoi, Y. Kadota, F. Ikeda, A universal solver for hyperbolic equations by cubic-polynomial interpolation II. Two- and three-dimensional solvers, Computer Physics Communications,**66**, 233242 (1991).

[33] T. Yabe, F. Xiao, T. Utsumi, Constrained interpolation profile method for multiphase analysis, J. Comput. Phys.,**169**, 556593 (2001).

[34] K. Yokoi, Numerical method for complex moving boundary problems in a Cartesian fixed grid, Phys. Rev. E., **65**, 055701(R) (2002).

[35] K. Yokoi, D. Vadillo, J. Hinch, I. Hutchings, Numerical studies of the influence of the dynamic contact angle on a droplet impacting on a dry surface, Phys. Fluids, **21**, 072102 (2009).

[36] K. Yokoi, Efficient implementation of THINC scheme: A simple and practical smoothed VOF algorithm, J. Comp. Phys. **226**, 1985-2002 (2007).

[37] K. Yokoi, A numerical method for free-surface flows and its application to droplet impact on a thin liquid layer, J. Sci. Comput., **35**, 372-396 (2008).

[38] K. Yokoi, Numerical studies of droplet splashing on a dry surface: triggering a splash with the dynamic contact angle, Soft Matter, **7**, 5120-5123 (2011).

[39] K. Yokoi, A practical numerical framework for free surface flows based on CLSVOF method, multi-moment methods and density-scaled CSF model20: Numerical simulations of droplet splashing, J. Comput. Phys., **232**, 252-271 (2013).

[40] K. Yokoi, A density-scaled continuum surface force model within a balanced force formulation, J. Comput. Phys., **278**, 221-228 (2014).

[41] K. Yokoi, R. Onishi, X. Deng, M. Sussman, Density-Scaled Balanced Continuum Surface Force Model with a Level Set Based Curvature Interpolation Technique, Int. J. Comput. Methods, DOI: 10.1142/S0219876216410048.

Table 1: $L_1$ errors in shock tube problems.

| | Sod | Lax |
|---|---|---|
| CDb | $2.25 \times 10^{-3}$ | $5.67 \times 10^{-3}$ |
| UPW | $2.30 \times 10^{-3}$ | $4.94 \times 10^{-3}$ |
| CDca | $2.24 \times 10^{-3}$ | $4.78 \times 10^{-3}$ |
| CDcc | $2.24 \times 10^{-3}$ | $4.47 \times 10^{-3}$ |
| CDbca | $2.21 \times 10^{-3}$ | $5.05 \times 10^{-3}$ |
| UPW-CDcc | $2.28 \times 10^{-3}$ | $4.61 \times 10^{-3}$ |
| UPW-CDbca | $2.27 \times 10^{-3}$ | $4.67 \times 10^{-3}$ |
| DP | N/A | $5.47 \times 10^{-3}$ |

Table 2: Summary of numerical results of incompressible flows. In the cavity flow problem, result by CSLR with central difference was slightly better than that by CSLR with mixed formulation.

| | Cavity flow | Droplet splashing |
|---|---|---|
| CSL2 with upwind | Fairly precise and not robust | Barely capture the phenomenon and not robust |
| CSL2 with central difference | Not robust | Not robust |
| CSLR with upwind | Fairly precise and robust | Capture the phenomenon and robust |
| CSLR with central difference | Precise and robust | Not robust |
| CSLR with mixed formulation | Precise and robust | Capture the phenomenon and robust |

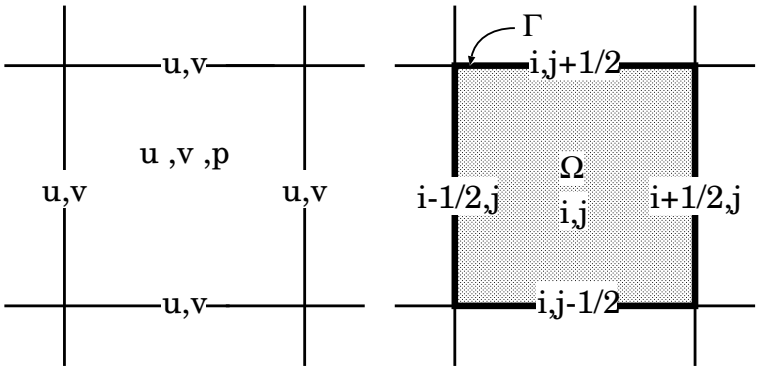


Figure 1: Schematic figure of the grid in two dimensional case. $u_{i,j}$ is the cell average and $u_{i-1/2,j}$, $u_{i+1/2,j}$, $v_{i,j-1/2}$ and $v_{i,j+1/2}$ are the boundary values.

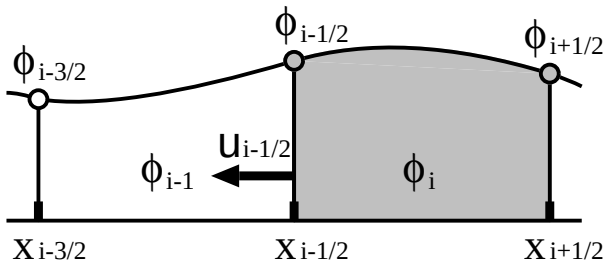


Figure 2: Schematic figure of the CIP-CSL2 method. $u_{i-1/2} < 0$ is assumed. The moments which are indicated by gray color ($\phi_{i-1/2}$, $\phi_i$ and $\phi_{i+1/2}$) are used to construct the quadratic interpolation function.

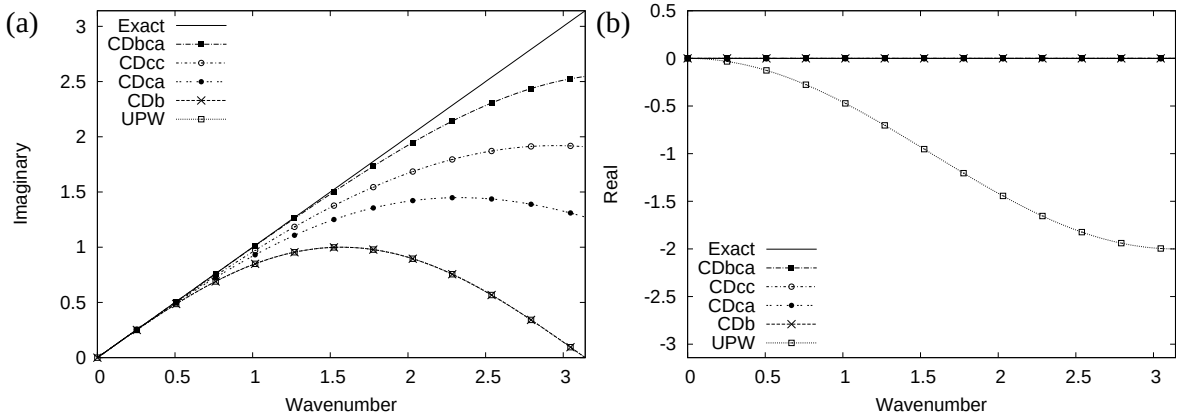


Figure 3: The formulations of the divergence term in Fourier analysis, (a) imaginary part and (b) real part.

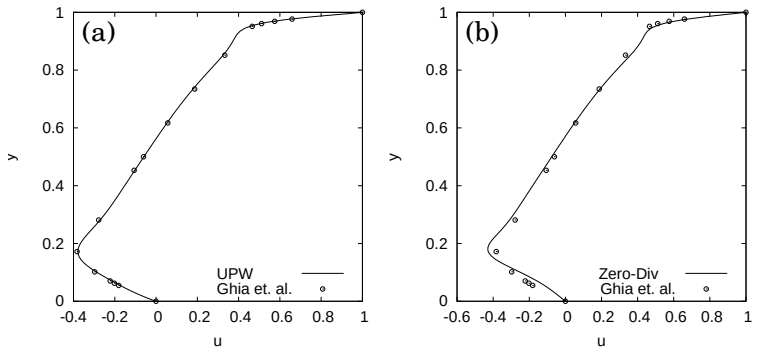


Figure 4: Numerical results of lid-driven cavity flow problem. CSL2 with UPW was used for (a). (b) is the result by CSL2 when the divergence term was ignored. The line and dot represent the numerical result and the solution by Ghia [2], respectively. A Cartesian grid of $100 \times 100$ was used.

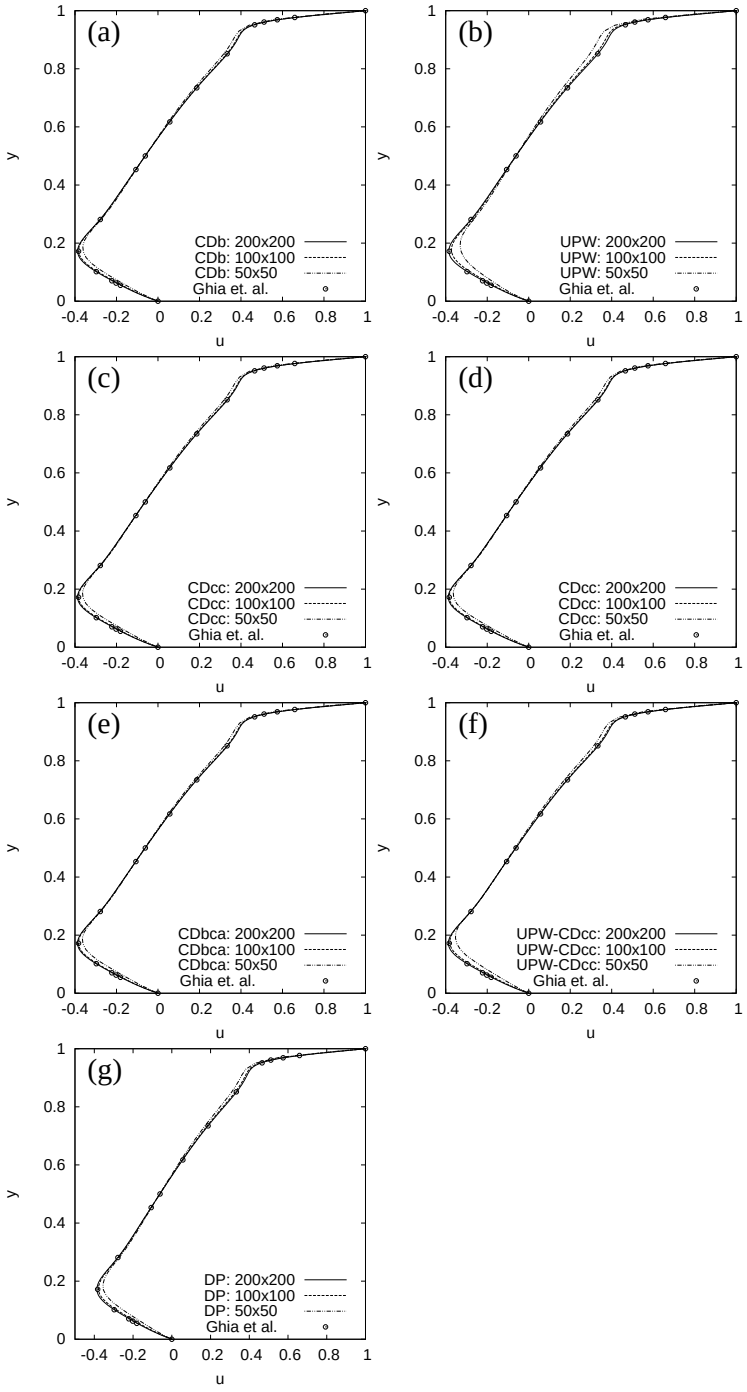


Figure 5: Numerical results of lid-driven cavity flow using six different formulations for the divergence term. Three different grid sizes ($50\times50$, $100\times100$ and $200\times200$) were used.

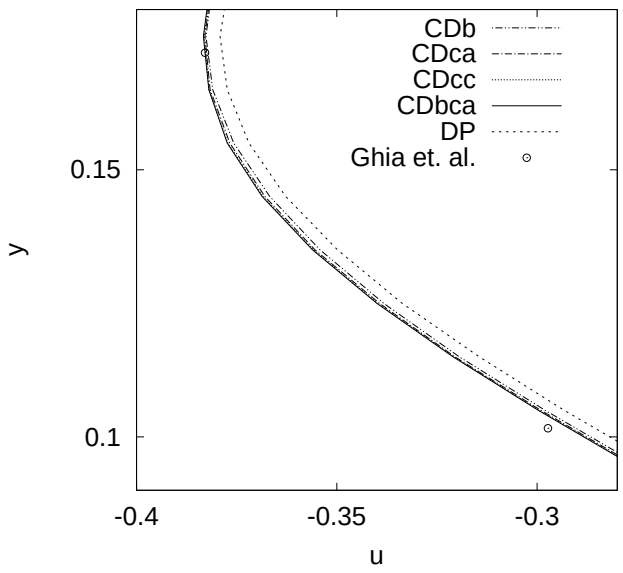


Figure 6: Comparison among numerical results by CSLR-CDb, CSLR-CDca, CSLR-CDcc, CSLR-CDbca and CSLR-DP. A Cartesian grid of $50 \times 50$ was used.

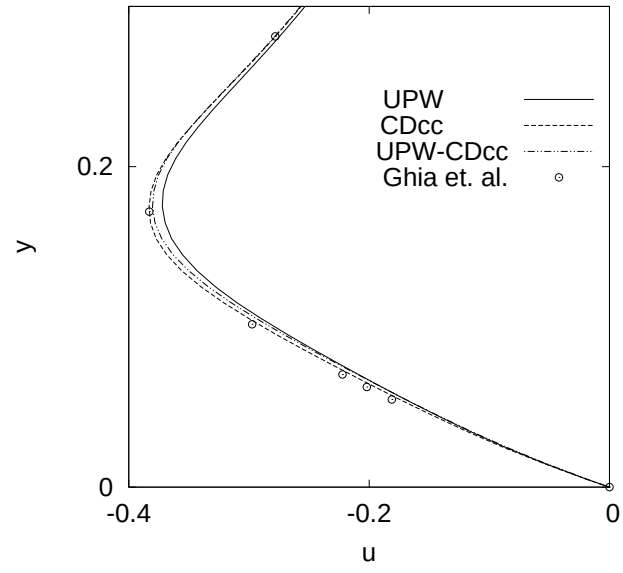


Figure 7: Comparison among numerical results by CSLR-UPW, CSLR-CDcc and CSLR-UPW-CDcc. A Cartesian grid of $100 \times 100$ was used.

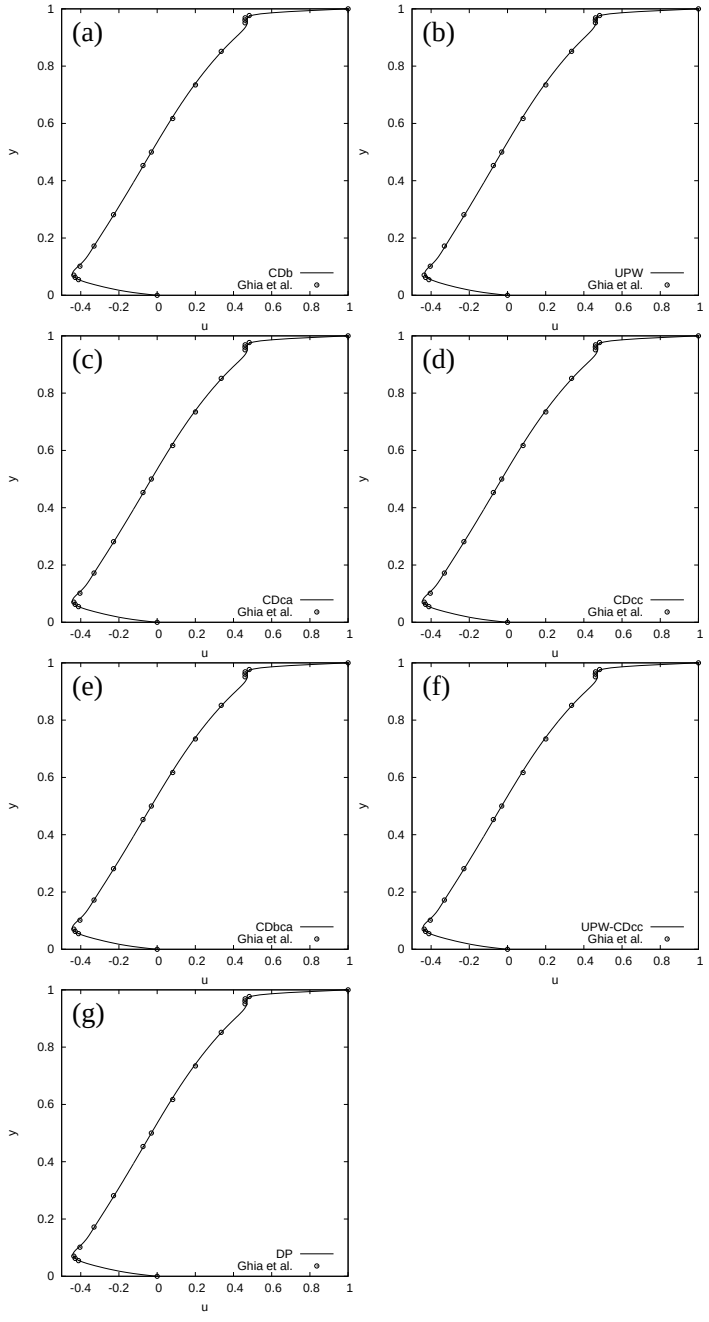


Figure 8: Numerical results of lid-driven cavity flow using six different formulations for the divergence term. Re = 5000. A Cartesian grid of $256 \times 256$ was used.

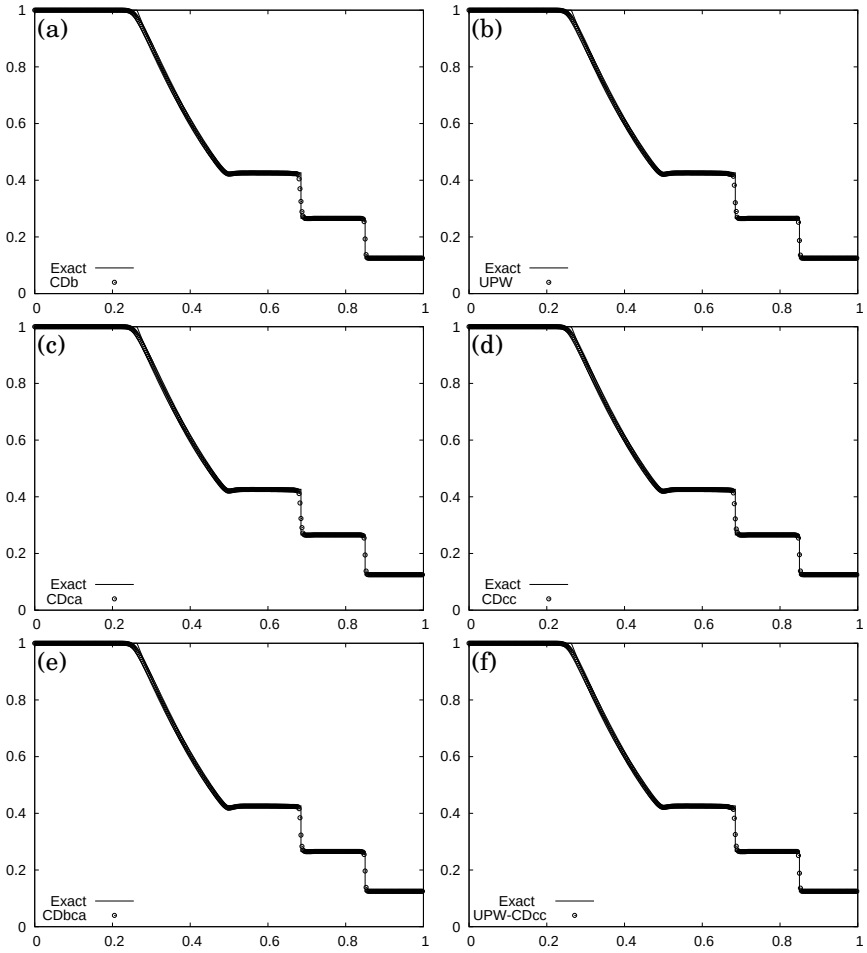


Figure 9: Numerical results of Sod's Problem. The dots show the density profile of numerical results. The line shows the exact solution.

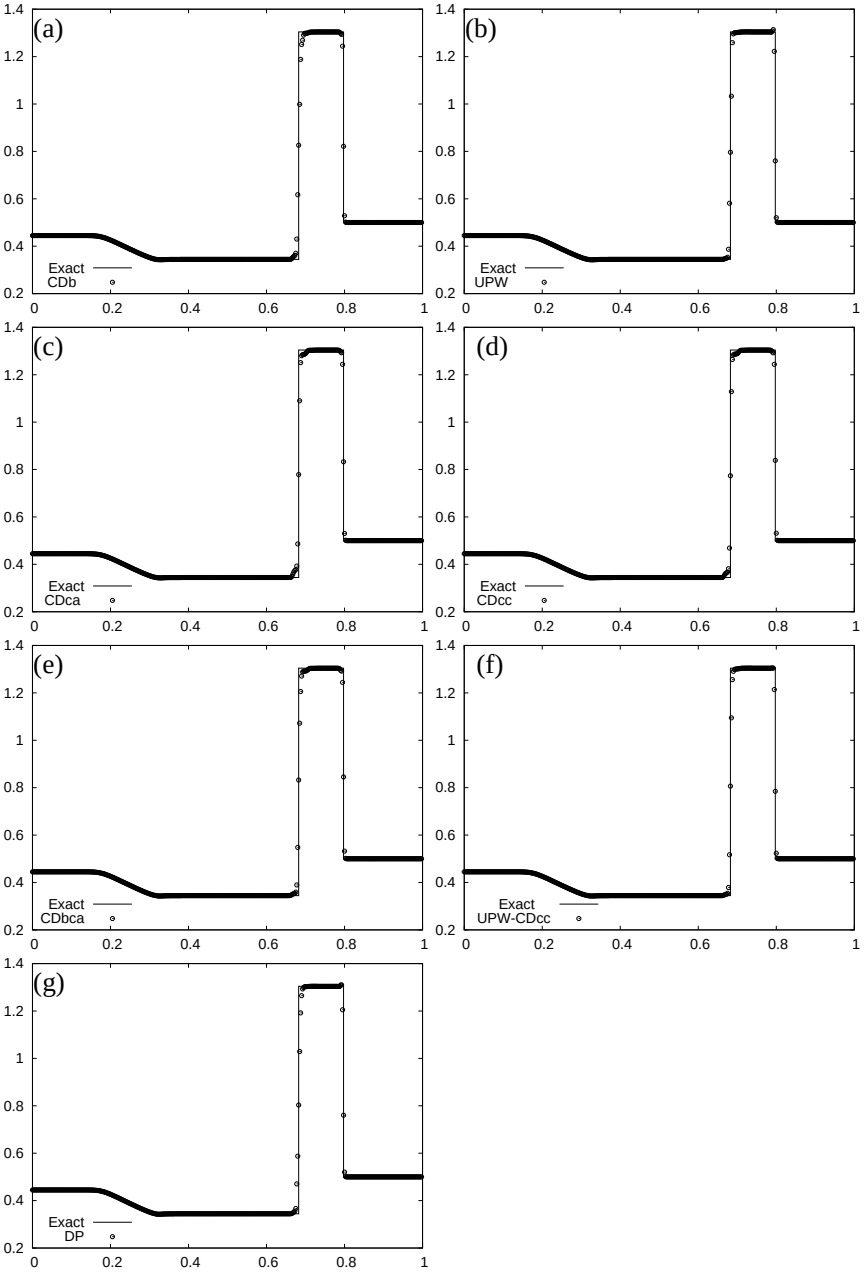


Figure 10: Numerical results of Lax's Problem. The dots show the density profile of numerical results. The line shows the exact solution.

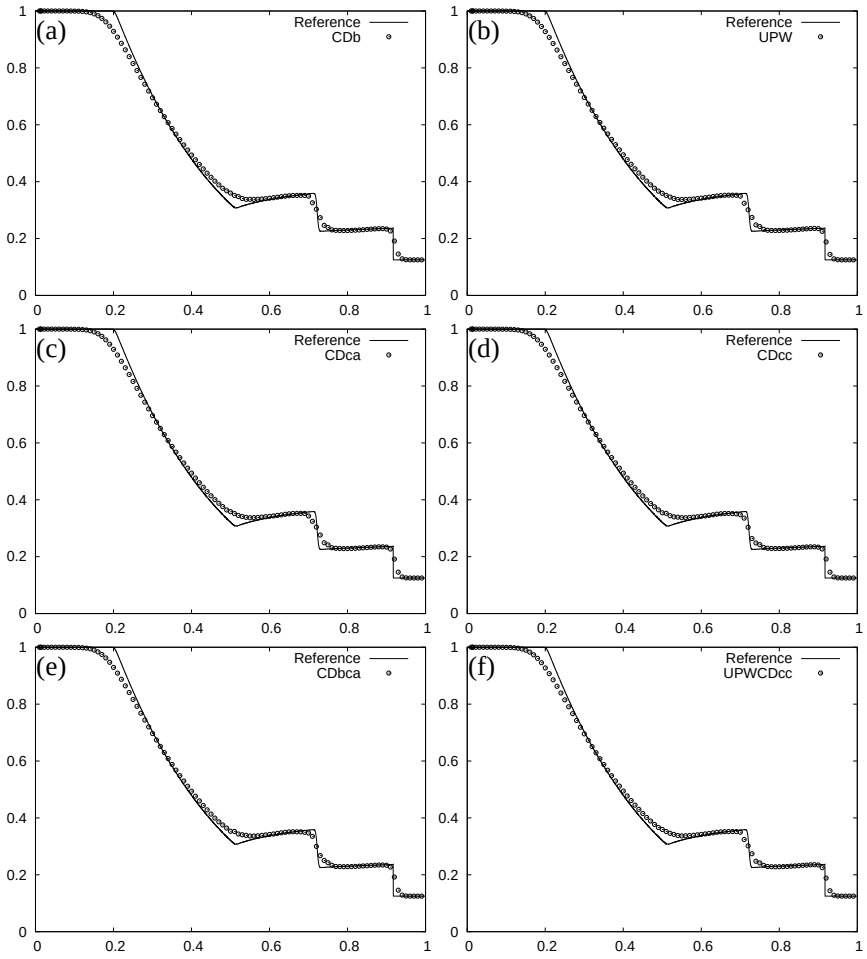


Figure 11: The density profiles of the 2-d explosion test at t=0.25 along the line of y = 0 . The dots represent numerical results by using six different formulations for the divergence term. The line represents the reference solution.

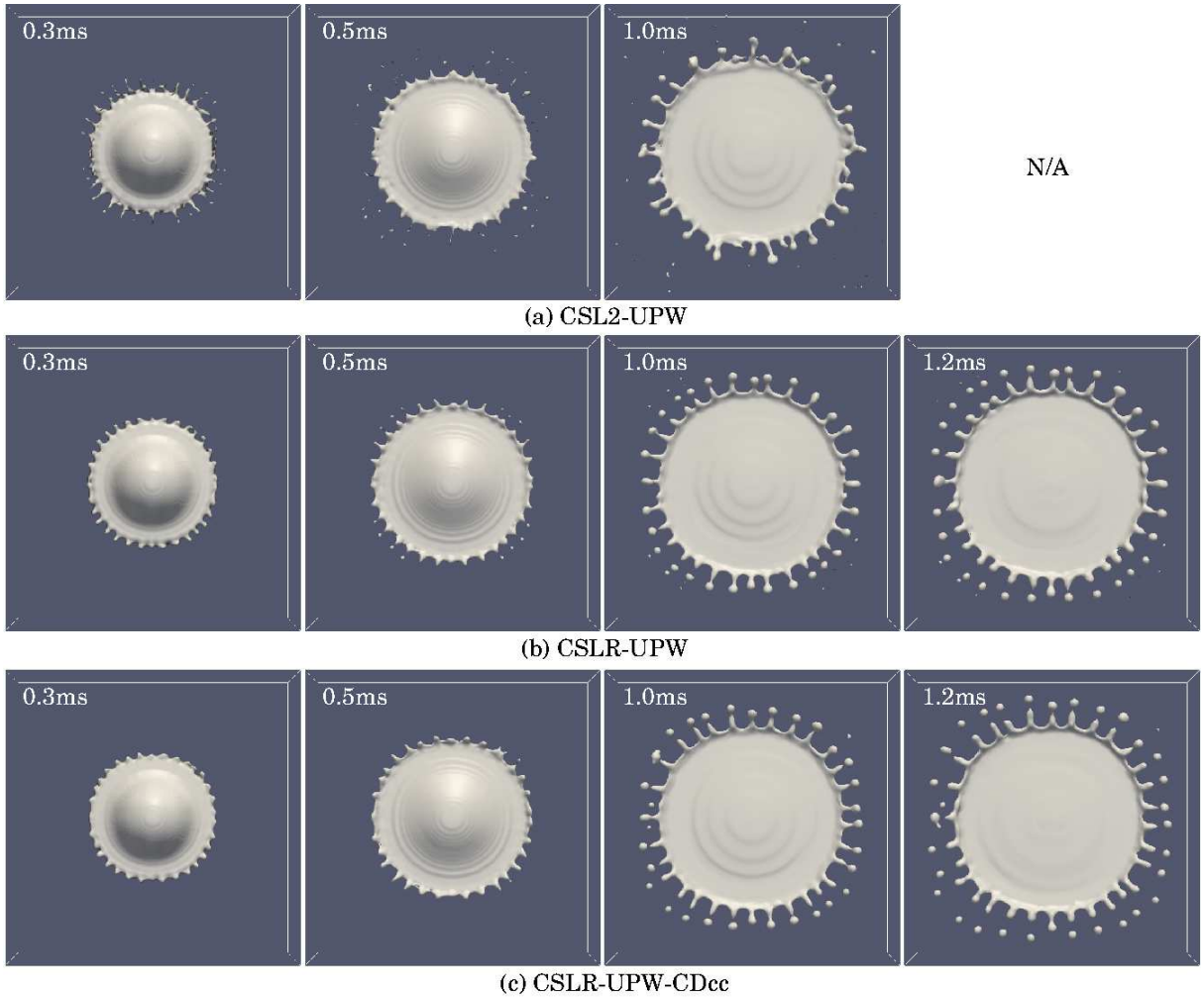


Figure 12: Numerical results of droplet splashing by CSL2-UPW (a), CSLR-UPW (b) and CSLR-UPW-CDcc (c). VSIAM3 with CSL2-UPW was not stable after around 1.1ms.

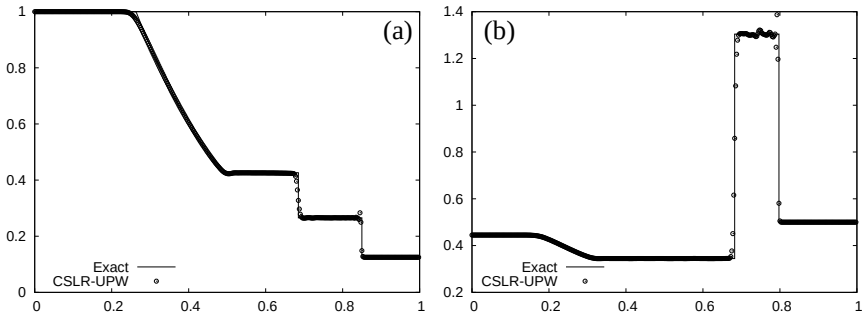


Figure 13: Numerica results of shock tube problems by CSLR-UPW , (a) Sod problem and (b) Lax problem. The dots show the density profile of numerical results. The line shows the exact solution.